Mass Fluctuation Kinetics: Analysis and Computation of Equilibria and Local Dynamics

Paul Azunre*, Carlos Gómez-Uribe†, George Verghese‡

June 16, 2011

Abstract

The mass fluctuation kinetics (MFK) model is a set of coupled ordinary differential equations approximating the time evolution of means and covariances of species concentrations in chemical reaction networks. It generalizes classical mass action kinetics (MAK), in which fluctuations around the mean are ignored. MFK may be used to approximate stochasticity in system trajectories when stochastic simulation methods are prohibitively expensive computationally. This paper presents a set of tools to aid in the analysis of systems within the MFK framework. A closed-form expression for the MFK Jacobian matrix is derived. This expression facilitates the computation of MFK equilibria and the characterization of the dynamics of small deviations from the equilibria (i.e., local dynamics). Software developed in MATLAB to analyze systems within the MFK framework is also presented. We outline a homotopy continuation method that employs the Jacobian for bifurcation analysis, i.e., to generate a locus of steady-state Jacobian eigenvalues corresponding to changing a chosen MFK parameter such as system volume or a rate constant. This method is applied to study the effect of small-volume stochasticity on local dynamics at equilibria in a pair of example systems, namely the formation and dissociation of an enzyme-substrate complex, and a genetic oscillator. For both systems, this study reveals volume regimes where MFK provides a quantitatively and/or qualitatively correct description of system behavior, and regimes where the MFK approximation is inaccurate. Moreover, our analysis provides evidence that decreasing volume from the MAK regime (infinite volume) has a destabilizing effect on system dynamics.

1 Introduction

Modeling the dynamics of species concentrations in chemical reaction networks at the cellular level is becoming a central task in systems biology applications (see, for instance, [1]). The traditional deterministic mass action kinetics (MAK) model describes the evolution of expected or mean concentrations of the different chemical species in a system through ordinary differential equations (ODEs). When molecules of some species occur in small numbers, a situation often observed at volumes comparable to that of the cell, deviations from MAK expected concentrations can become significant, and more refined models are then needed to capture the inherent stochasticity of trajectories [2].

*EECS Department, Room 13-3029, Massachusetts Institute of Technology, Cambridge, MA 02139, USA (azunre@mit.edu).

†Netflix Inc., 100 Winchester Circle, Los Gatos, CA 95032 (cgomez@alum.mit.edu).

‡EECS Department, Room 10-140K, Massachusetts Institute of Technology, Cambridge, MA 02139, USA (verghese@mit.edu).

A widely used approach to describe the stochasticity of trajectories is the linear noise approximation [3] [4], which estimates all covariances in addition to the means, with the means being those computed by MAK. Because the coupling of the covariances back to the means is not taken into account, this approximation becomes increasingly inaccurate at small system volumes.

A more accurate but also more involved approach to describe the stochasticity of trajectories is to use the chemical master equation (CME), which describes the evolution of the joint probability distribution of molecule numbers [2]. The CME cannot be solved analytically most of the time, due to the high number of possible system states, which is the product of the feasible number of molecules for each of the chemical species in the system. As a consequence, stochastic simulation methods, such as Gillespie's widely used stochastic simulation algorithm (SSA) [2], are often used to draw a sample of trajectories from the CME, and statistics of the sample (means, covariances, etc.) are then used to describe stochasticity. Simulation approaches are unfortunately often computationally very expensive, so further approximations have been developed.

The mass fluctuation kinetics (MFK) model is an approximation for the CME that describes stochasticity deterministically through coupled ODEs, one for each concentration mean and covariance [5] [6]. The MFK model is derived under the 'moment closure' assumption that central moments of third-order are negligible (a reasonable assumption when, for instance, propensity functions — defined in the next section — are quadratic, and the state distributions are approximately symmetric). This is related to the method described in [7] in a broader setting, where all cumulants of order greater than two are set to zero (thereby obtaining a normal distribution). The ability of MFK to capture efficiently the stochasticity in certain regimes of a range of systems, with accuracy comparable to the stochastic simulation methods but at a lower computational cost, has been demonstrated [5]. A detailed comparative analysis of popular moment closure methods (including MFK) can be found in [8]. A moment closure approach based on matching time derivatives between exact and approximate moment equations is derived in [8] and shown also to be the most accurate of the various methods (especially when molecule numbers are small), though at the expense of using additional nonlinear terms.

This paper presents a set of tools to aid in the analysis of systems within the MFK framework. Some necessary background is introduced in Section 2. A closed-form expression for the MFK Jacobian matrix is derived in Section 3 and the Appendix. We show that the expression facilitates the computation of MFK equilibria and the characterization of the dynamics of small deviations from the equilibria (i.e., local dynamics). We outline a homotopy continuation method that employs the Jacobian for bifurcation analysis, i.e., to generate a locus of steady-state Jacobian eigenvalues corresponding to changing a chosen MFK parameter such as system volume or a rate constant. Software developed in MATLAB to analyze systems within the MFK framework is presented in Section 4. The homotopy continuation method is then applied to study the effect of small-volume stochasticity on local dynamics at equilibria in a pair of example systems, by focusing on the eigenvalue locus corresponding to decreasing system volume. More specifically, the systems considered are the formation and dissociation of an enzyme-substrate complex, and a genetic oscillator. For both systems, this study reveals volume regimes where MFK provides a quantitatively and/or qualitatively correct description of system behavior, and regimes where the MFK approximation is inaccurate. Moreover, our analysis provides evidence that decreasing volume from the MAK regime (infinite volume) has a destabilizing effect on system dynamics.

2 Background

2.1 CME and MAK

In what follows, $\mathbb{Z}$ denotes the integers and $\mathbb{R}$ the real numbers, with the dimensions of matrices with entries in $\mathbb{Z}$ or $\mathbb{R}$ being indicated by superscripts. Consider molecules of n chemical species, $\{X_i\}_{i=1}^n$, interacting through L reactions of the form

$$\left\{ R_l : \sum_{i=1}^{n} \underline{s}_{il} X_i \xrightarrow{k_l} \sum_{i=1}^{n} \overline{s}_{il} X_i \right\}_{l=1}^{L}, \tag{1}$$

in a constant volume ν. The parameter k_l is the rate constant for R_l. The stoichiometric coefficient of X_i in R_l, defined as the change in the number x_i of molecules of X_i upon each firing of R_l, is calculated as $s_{il} = \overline{s}_{il} - \underline{s}_{il}$. Stoichiometric coefficients are grouped into the stoichiometry vectors $\{\mathbf{s}_l \in \mathbb{Z}^n\}_{l=1}^L$ and further into the system's stoichiometry matrix $\mathbf{S} \in \mathbb{Z}^{n \times L}$. System size is denoted as $\Omega = A\nu$, where A is Avogadro's number. The molecule numbers $\{x_i\}_{l=1}^n$ for all species at a particular time t are grouped in a state vector $\mathbf{x}(t) \in \mathbb{Z}^n$, and concentrations are computed in units of moles per unit volume as $\mathbf{y}(t) = \frac{\mathbf{x}(t)}{\Omega} \in \mathbb{R}^n$. We are interested in the evolution of concentrations with respect to time.

Propensity functions $\{a_l(\mathbf{x}(t))\}_{l=1}^L$ for reactions $\{R_l\}_{l=1}^L$ are defined such that the respective firing probabilities for the reactions are $\{a_l(\mathbf{x}(t))dt\}_{l=1}^L$ within the next infinitesimal interval dt, with each reaction considered in isolation. This establishes a Markov process model for the system of chemical reactions, with state $\mathbf{x}(t) \in \mathbb{Z}^n$ and exponential state transition rates $\{a_l(\mathbf{x}(t))\}_{l=1}^L$. With $P(\mathbf{x}(t))$ denoting the probability of obtaining state $\mathbf{x}(t)$ conditioned on some initial state $\mathbf{x}(0)$, the forward Kolmogorov equation [9] for the Markov process is written as

$$\frac{dP(\mathbf{x}(t))}{dt} = \sum_{l=1}^{L} \left[P(\mathbf{x}(t) - \mathbf{s}_l) a_l(\mathbf{x}(t) - \mathbf{s}_l) - P(\mathbf{x}(t)) a_l(\mathbf{x}(t)) \right]. \tag{2}$$

This is the chemical master equation (CME). It is composed of one differential equation for each possible state.

The deterministic MAK equations for the evolution of species concentrations $\mathbf{y}(t)$ follow from the CME in the limit of large Ω, and are written as

$$\frac{d\mathbf{y}(t)}{dt} = \sum_{l=1}^{L} \mathbf{s}_l \lim_{\Omega \to \infty} \left\{ \frac{a_l(\mathbf{y}(t)\Omega)}{\Omega} \right\} = \sum_{l=1}^{L} \mathbf{s}_l \bar{\rho}_l(\mathbf{y}(t)), \tag{3}$$

under the assumption that the indicated limit exists [2]. The deterministic macroscopic reaction rates $\{\bar{\rho}_l(\mathbf{y}(t))\}_{l=1}^L$ are proportional to the products of concentrations of their respective reactants in $\{R_l\}_{l=1}^L$. These deterministic equations are not suitable for capturing system dynamics when stochasticity is a significant feature of trajectories, as they ignore fluctuations around the means and the effect of fluctuations on the means themselves.

2.2 MFK

The mass fluctuation kinetics (MFK) model captures stochasticity deterministically through coupled ODEs that approximate the evolution of all concentration means and covariances [5] [6], by assuming third-order central moments to be negligible. MFK is significantly less computationally

expensive than simulation-based approaches. The introduction of covariances, and their coupling to the means, enables it to capture dynamics better than MAK, which only tracks the means, and better than the linear noise approximation [3] [4], which ignores the effect of covariances on the means. The MFK rate equations can also be shown to follow (under the same moment-closure assumption) from the evolution of generating functions obtained from the CME [8], [10], [11], [12]. This derivation approach differs from the approach taken in [5] and [6], and provides a systematic way of extending MFK to central moments of arbitrarily higher order.

For notational convenience, the dependence of $\mathbf{x}(t)$, $\mathbf{y}(t)$, $P(\mathbf{x}(t))$ and other quantities on t is henceforth made implicit, with the variables respectively referred to as $\mathbf{x}$, $\mathbf{y}$ and $P(\mathbf{x})$. We define the microscopic reaction rates as appropriately scaled propensities, written as

$$\left\{ \rho_l(\mathbf{y}) \equiv \frac{a_l(\mathbf{y}\Omega)}{\Omega} \right\}_{l=1}^{L}, \tag{4}$$

being stacked into a single microscopic rate vector as

$$\boldsymbol{\rho}(\mathbf{y}) = \left[\begin{array}{ccc} \rho_1(\mathbf{y}) & \cdots & \rho_L(\mathbf{y}) \end{array} \right]^T. \tag{5}$$

The mean concentration vector is defined as

$$\boldsymbol{\mu} = \frac{1}{\Omega} \langle \mathbf{x} \rangle, \tag{6}$$

with $\langle \cdot \rangle$ denoting expectation taken over $P(\mathbf{x})$. The concentration covariance matrix is defined as

$$\mathbf{V} = \frac{1}{\Omega^2} \left\langle (\mathbf{x} - \boldsymbol{\mu}) (\mathbf{x} - \boldsymbol{\mu})^T \right\rangle. \tag{7}$$

Assuming that central moments of order three are negligible, the following equation may then be derived from (2) for the evolution of the mean vector:

$$\begin{aligned} \frac{d\boldsymbol{\mu}}{dt} &= \mathbf{S} \left(\boldsymbol{\rho}(\boldsymbol{\mu}) + \frac{1}{2} \frac{d^2 \boldsymbol{\rho}}{d\mathbf{y} d\mathbf{y}} (\boldsymbol{\mu}) \, vec\{\mathbf{V}\} \right) && (8) \\ &= \mathbf{S}\mathbf{r}. && (9) \end{aligned}$$

Here, $\mathbf{r}$ denotes the quantity in parentheses in (8), and $vec\{\mathbf{V}\}$ denotes the vectorization of $\mathbf{V}$, the column vector formed by stacking its columns [13]. Similarly, the following equation may be derived from (2) for the evolution of the covariance matrix:

$$\begin{aligned} \frac{d\mathbf{V}}{dt} &= \mathbf{S} \left(\frac{d\boldsymbol{\rho}}{d\mathbf{y}} (\boldsymbol{\mu}) \right) \mathbf{V} + \mathbf{V} \left(\frac{d\boldsymbol{\rho}}{d\mathbf{y}} (\boldsymbol{\mu}) \right)^T \mathbf{S}^T + \frac{1}{\Omega} \mathbf{S} \, diag\{\mathbf{r}\} \, \mathbf{S}^T \\ &= \mathbf{M}\mathbf{V} + \mathbf{V}\mathbf{M}^T + \frac{1}{\Omega} \mathbf{S} \boldsymbol{\Lambda} \mathbf{S}^T. && (10) \end{aligned}$$

Here,

$$\mathbf{M} = \mathbf{S} \frac{d\boldsymbol{\rho}}{d\mathbf{y}} (\boldsymbol{\mu}) \tag{11}$$

and

$$\boldsymbol{\Lambda} = diag\{\mathbf{r}\}, \tag{12}$$

which is the diagonal matrix whose diagonal entries are the components of $\mathbf{r}$. Equations (9) and (10) constitute the MFK model. This model is exact for systems described by quadratic propensity functions, and whose state distributions are symmetric (e.g., Gaussian). Since state distributions are seldom symmetric, this is almost always only an approximation.

Setting $\Omega = \infty$ and initializing $\mathbf{V}(0) = \mathbf{0}$ makes (10) evaluate to $\mathbf{0}$, implying that this is an equilibrium regime for $\mathbf{V}$. Moreover, (9) and (3) are then equivalent, so $\frac{d\boldsymbol{\mu}}{dt}$ in this case captures MAK dynamics. We thus specify the MAK regime as $\{\Omega, \mathbf{V}(0)\} = \{\infty, \mathbf{0}\}$.

2.3 Quadratic Propensities

The assumption that reactions among three or more reactant molecules are rare allows us to express each $\rho_l(\mathbf{y})$ as a quadratic function of $\mathbf{y}$. We use the standard notation $\mathbf{A}\otimes\mathbf{B}$ to denote the Kronecker product [13] of the matrices $\mathbf{A}$ and $\mathbf{B}$, i.e., the block-matrix whose (i,j)th block is $a_{ij}\mathbf{B}$, where a_{ij} is the element of $\mathbf{A}$ in its ith row and jth column. Every $\rho_l(\mathbf{y})$ may then be expressed in the quadratic form

$$\rho_l(\mathbf{y}) = k_l\left(b_l + \mathbf{c}_l^T\mathbf{y} + \mathbf{y}^T\mathbf{D}_l\mathbf{y}\right) = k_l\left(b_l + \mathbf{c}_l^T\mathbf{y} + vec\{\mathbf{D}_l\}^T(\mathbf{y}\otimes\mathbf{y})\right). \tag{13}$$

Each b_l, $\mathbf{c}_l$ and $\mathbf{D}_l$ can be found by inspection from the specifications of the reactions (see Example 1 below, also Appendix A of [5], for more details). We define matrices

$$\mathbf{D} = \left[\begin{array}{ccc} vec(\mathbf{D}_1)| & \ldots & |vec(\mathbf{D}_L) \end{array}\right], \tag{14}$$

$$\mathbf{K} = diag\{k_1,\ldots,k_L\}, \tag{15}$$

$$\mathbf{C} = \left[\begin{array}{ccc} \mathbf{c}_1| & \cdots & |\mathbf{c}_L \end{array}\right], \tag{16}$$

and find $\mathbf{r}$ in (8), (9) to be

$$\mathbf{r} = \mathbf{K}\left(\mathbf{b} + \mathbf{C}^T\boldsymbol{\mu} + \mathbf{D}^T(\boldsymbol{\mu}\otimes\boldsymbol{\mu}) + \mathbf{D}^T vec\{\mathbf{V}\}\right), \tag{17}$$

where

$$\mathbf{b} = \left[\begin{array}{ccc} b_1 & \cdots & b_L \end{array}\right]^T, \tag{18}$$

and $\mathbf{M}$ in (11) to be

$$\mathbf{M} = \mathbf{S}\frac{d\boldsymbol{\rho}}{d\mathbf{y}}(\boldsymbol{\mu}) = \mathbf{SK}\left(\mathbf{C}^T + 2\mathbf{D}^T(\mathbf{I}_n\otimes\boldsymbol{\mu})\right). \tag{19}$$

Here, $\mathbf{I}_n$ denotes the n-by-n identity matrix.

2.4 Illustrative Example

The following simple example system will be used to illustrate key concepts in the remainder of the paper. The MFK and MAK descriptions are contrasted.

Example 1 (**MFK for Complex Formation/Dissociation**) Consider the system described by substrate S interacting with enzyme E to form complex C, written as the reversible reaction

$$E + S \underset{k_2}{\overset{k_1}{\rightleftharpoons}} C. \tag{20}$$

Stoichiometry vectors $\mathbf{s}_1$ and $\mathbf{s}_2$ are grouped into the stoichiometry matrix $\mathbf{S}$ as

$$\mathbf{S} = \left[\begin{array}{cc} \mathbf{s}_1 & \mathbf{s}_2 \end{array}\right] = \begin{array}{c} \\ E \\ S \\ C \end{array}\begin{array}{c} \begin{array}{cc} R_1 & R_2 \end{array} \\ \left[\begin{array}{cc} -1 & 1 \\ -1 & 1 \\ 1 & -1 \end{array}\right] \end{array}. \tag{21}$$

One molecule of E is consumed by R_1 to produce one molecule of C, which is reversed exactly by R_2. Thus, $\pi_1 = y_E + y_C$ must be conserved. Similar reasoning concludes that $\pi_2 = y_S + y_C$ is also conserved. Thus, the concentration of only one species, C, needs to be tracked, so effectively $\mathbf{S} = [1, -1]$, the last row in (21). To determine the MFK evolution equations, microscopic rates

are written for R_1 and R_2 (using the fact that for both reactions the rates are proportional to the products of the concentrations of the reactants) as

$$\begin{aligned} \rho_1(y_C) &= k_1 y_E y_S = k_1 (\pi_1 - y_C)(\pi_2 - y_C) \\ &= k_1 \left[\pi_1\pi_2 - (\pi_1 + \pi_2) y_C + y_C^2\right], \qquad (22) \\ \rho_2(y_C) &= k_2 y_C. \qquad (23) \end{aligned}$$

The microscopic rate parameters are obtained by direct comparison with (13) as

$$\begin{array}{lll} b_1 = \pi_1\pi_2, & \mathbf{c}_1 = -(\pi_1 + \pi_2), & \mathbf{D}_1 = 1, \\ b_2 = 0, & \mathbf{c}_2 = 1, & \mathbf{D}_2 = 0. \end{array} \qquad (24)$$

Thus

$$\mathbf{r} = \left[\begin{array}{c} k_1\left(\pi_1\pi_2 - (\pi_1 + \pi_2)\mu_C + \mu_C^2 + \sigma_{CC}\right) \\ k_2\mu_C \end{array}\right]. \qquad (25)$$

The MFK evolution equation for μ_C, the expected concentration of C, with the familiar MAK portion indicated by the underbrace, is therefore

$$\frac{d\mu_C}{dt} = \underbrace{k_1\left[\pi_1\pi_2 - (\pi_1 + \pi_2)\mu_C + \mu_C^2\right] - k_2\mu_C}_{\text{MAK}} + k_1\sigma_{CC} \qquad (26)$$

(we have omitted the time argument t on μ_C and σ_{CC}, for notational simplicity). The matrix $\mathbf{M}$ (in this case, scalar) is

$$\mathbf{M} = k_1\left[2\mu_C - (\pi_1 + \pi_2)\right] - k_2. \qquad (27)$$

The MFK evolution equation for σ_{CC}, the variance of C, is thus

$$\begin{aligned} \frac{d\sigma_{CC}}{dt} &= 2\sigma_{CC}\left(k_1\left[2\mu_C - (\pi_1 + \pi_2)\right] - k_2\right) \\ &\quad + \frac{1}{\Omega}\left(k_1\left[\pi_1\pi_2 - (\pi_1 + \pi_2)\mu_C + \mu_C^2 + \sigma_{CC}\right] + k_2\mu_C\right). \qquad (28) \end{aligned}$$

3 MFK Jacobian Matrix

The goal of studying the properties of the local dynamics at MFK equilibria motivates establishing a closed-form expression for the MFK Jacobian matrix, which is done in this section. While this matrix can in principle be found via symbolic differentiation for any particular system, that can be more unwieldy and less computationally efficient than deriving and using a general closed-form expression [14]. The Jacobian matrix governs the dynamics of small deviations from a nominal solution or equilibrium point. It contains the partial derivatives of the MFK evolution equations with respect to each state variable. Knowing the Jacobian can facilitate computation of equilibrium points. When evaluated at a constant equilibrium point, its eigenvalues indicate the degree of local stability (or instability) around the equilibrium. The Jacobian can also be applied to bifurcation analysis using a homotopy continuation method, as is outlined in this section.

We begin by writing MFK in conventional state-space form. For this purpose, we will need to vectorize MFK with $vec\{\cdot\}$. Because $\mathbf{V}$ is symmetric, we will also need the half-vectorization operator $vech\{\cdot\}$, the column-wise stacking of only the lower-triangular part of a matrix [13], to eliminate redundancy in expressions. The relationship between the two operators is captured by

the (nonunique) selection and (unique) duplication binary matrices [13], $\mathbf{E}_n$ and $\mathbf{F}_n$ respectively, through

$$vech\{\mathbf{V}\} = \mathbf{E}_n vec\{\mathbf{V}\}, \tag{29}$$
$$vec\{\mathbf{V}\} = \mathbf{F}_n vech\{\mathbf{V}\}. \tag{30}$$

The Appendix shows that the MFK description can now be rewritten as a conventional state-space representation of the form

$$\frac{d\mathbf{z}}{dt} = \mathbf{g}(\mathbf{z}), \tag{31}$$

where the state vector is

$$\mathbf{z} = \begin{bmatrix} \boldsymbol{\mu} \\ vech\{\mathbf{V}\} \end{bmatrix} = \begin{bmatrix} \boldsymbol{\mu} \\ \mathbf{v} \end{bmatrix} \in \mathbb{R}^{\frac{n(n+3)}{2}}, \tag{32}$$

with $\mathbf{v}$ denoting $vech\{\mathbf{V}\}$, $\mathbf{z}$ being a vector of dimension $\eta = \frac{n(n+3)}{2}$, and the function $\mathbf{g}$ being explicitly described in the Appendix (see, in particular, (46)).

The Jacobian of interest to us is now defined as

$$\begin{aligned} \mathbf{J}(\mathbf{z}) &= \frac{d\mathbf{g}(\mathbf{z})}{d\mathbf{z}} \in \mathbb{R}^{\eta\times\eta} \\ &= \begin{bmatrix} \frac{\partial}{\partial\boldsymbol{\mu}}\left\{\frac{d\boldsymbol{\mu}}{dt}\right\} & \frac{\partial}{\partial\mathbf{v}}\left\{\frac{d\boldsymbol{\mu}}{dt}\right\} \\ \frac{\partial}{\partial\boldsymbol{\mu}}\left\{\frac{d\mathbf{v}}{dt}\right\} & \frac{\partial}{\partial\mathbf{v}}\left\{\frac{d\mathbf{v}}{dt}\right\} \end{bmatrix}. \end{aligned} \tag{33}$$

The four terms of this block matrix are derived explicitly in the Appendix, resulting in (54)-(57). Note that in (31) and (33), time dependence of the various terms has been been made implicit for notational simplicity.

3.1 Application to Computing Equilibria and Local Stability

An equilibrium $\bar{\mathbf{z}}$ of the MFK model (31) is characterized by $\mathbf{g}(\bar{\mathbf{z}}) = 0$. Newton's method [15] may be implemented to find equilibria using the Jacobian, as is done in the software tool described in the next section. At the i^{th} iteration, the definition of the Jacobian and a first-order Taylor expansion establish

$$\mathbf{J}\left(\mathbf{z}^i\right)\left(\mathbf{z}^{i+1} - \mathbf{z}^i\right) \approx \mathbf{g}(\mathbf{z}^{i+1}) - \mathbf{g}(\mathbf{z}^i). \tag{34}$$

Here, $\mathbf{z}^{i+1}$ is the next (and one hopes better) approximation for the equilibrium, so we set $\mathbf{g}(\mathbf{z}^{i+1})$ to 0, thus obtaining the iteration

$$\mathbf{z}^{i+1} = \mathbf{z}^i - \left(\mathbf{J}\left(\mathbf{z}^i\right)\right)^{-1}\mathbf{g}(\mathbf{z}^i). \tag{35}$$

This is started at some initial guess $\mathbf{z}_0$ and performed until some convergence tolerance is satisfied.

The real parts of the Jacobian eigenvalues at the equilibrium specify whether the equilibrium is locally stable or not. In particular, if the real parts of the eigenvalues are all negative, then the equilibrium is locally stable. Otherwise, the equilibrium is not locally stable.

3.2 Application to Bifurcation Analysis

It may be desirable to perform bifurcation analysis of the MFK model, i.e., to track a locus of steady-state Jacobian eigenvalues corresponding to changing a given MFK parameter. Such analysis can reveal parameter regimes where the model exhibits desired steady-state behavior (e.g., stability, oscillation, etc). In what follows, a special case of this analysis is outlined, by focusing on system size as a parameter to study the effect of small-volume stochasticity on steady-state local dynamics. This is readily generalizable to other MFK parameters (e.g., one of the rate constants k_l, in place of system size). A bifurcation analysis method for the linear noise approximation, which is conceptually similar to the method developed here but which differs in many details of its development, is described in [16].

If Ω is made smaller, and initial concentrations are kept the same, then molecule numbers must decrease. We expect stochasticity to then become increasingly important. Insight into the effect of small-volume stochasticity on steady-state stability can then be obtained by studying local stability along a sequence of MFK equilibria corresponding to decreasing Ω. We take a homotopy continuation approach [15], finding an MFK equilibrium $\bar{\mathbf{z}}_{MAK}$ in the MAK regime and tracking a sequence of MFK equilibria with decreasing Ω. The Jacobian is evaluated along this sequence, and local stability is inferred by analyzing its eigenvalues.

We denote inverse system size as $\mho = \frac{1}{\Omega}$ (which can be read as 'mho') and make explicit the dependence of $\mathbf{g}(\mathbf{z})$ on volume by rewriting it as $\mathbf{g}(\mathbf{z}, \mho)$. Performing a first-order Taylor expansion of $\mathbf{g}(\mathbf{z}, \mho)$ around $(\bar{\mathbf{z}}_1, \mho_1)$, where $\bar{\mathbf{z}}_1$ is an equilibrium realized at $\mho_1$, yields

$$\mathbf{g}(\mathbf{z}, \mho) \approx \overbrace{\mathbf{g}(\bar{\mathbf{z}}_1, \mho_1)}^{\mathbf{0}} + \overbrace{\frac{\partial \mathbf{g}}{\partial \mathbf{z}}(\bar{\mathbf{z}}_1, \mho_1)}^{\mathbf{J}(\bar{\mathbf{z}}_1, \mho_1)} (\mathbf{z} - \bar{\mathbf{z}}_1) + \frac{\partial \mathbf{g}}{\partial \mho}(\bar{\mathbf{z}}_1, \mho_1)(\mho - \mho_1). \tag{36}$$

Letting $(\bar{\mathbf{z}}_2, \mho_2)$ be another similar equilibrium point sufficiently close to $(\bar{\mathbf{z}}_1, \mho_1)$, we find from (36) that

$$\mathbf{g}(\bar{\mathbf{z}}_2, \mho_2) = \mathbf{0} \approx \mathbf{J}(\bar{\mathbf{z}}_1, \mho_1)(\bar{\mathbf{z}}_2 - \bar{\mathbf{z}}_1) + \frac{\partial \mathbf{g}}{\partial \mho}(\bar{\mathbf{z}}_1, \mho_1)(\mho_2 - \mho_1). \tag{37}$$

The remaining partial derivative is obtained from (9) and (46) in the Appendix as

$$\frac{\partial \mathbf{g}(\mathbf{z}, \mho)}{\partial \mho} = \begin{bmatrix} \mathbf{0} \\ \mathbf{E}_n(\mathbf{S} * \mathbf{S})\mathbf{r} \end{bmatrix}, \tag{38}$$

where $*$ denotes the columnwise Kronecker product, also known as the Khatri-Rao product [17]. It follows from (37) that

$$\frac{d\bar{\mathbf{z}}}{d\mho} = -(\mathbf{J}(\bar{\mathbf{z}}, \mho))^{-1} \begin{bmatrix} \mathbf{0} \\ \mathbf{E}_n(\mathbf{S} * \mathbf{S})\mathbf{r} \end{bmatrix}, \tag{39}$$

where $\mathbf{r}$ is evaluated at $\bar{\mathbf{z}}$. This differential equation is integrated over a specified range of $\mho$ to yield a sequence of equilibria. We start this sequence at $\{\mho, \mathbf{V}(0)\} = \{0, \mathbf{0}\}$, which corresponds to the MAK equilibrium $\bar{\mathbf{z}}_{MAK}$, and end it at some specified final $\mho$ value. At each $\{\bar{\mathbf{z}}, \mho\}$ pair, the Jacobian is evaluated and its eigenvalues computed.

The effect of small-volume stochasticity on local dynamics at equilibria is studied in the next section for a pair of example systems, using the outlined method.

4 Numerical Study

To automate the analysis of systems within the MFK framework, we have written some software in MATLAB. The software relies on the SimBiology MATLAB toolbox for system description via

a convenient graphical user interface and conservation analysis. It uses the Symbolic Math toolbox for building the MFK model description of a given system and conveniently displaying it in human-readable analytic form (for sufficiently simple systems). An implementation of Gillespie's stochastic simulation algorithm is included, for use as an adjunct to MFK computations, as illustrated in our examples. The examples presented here and in [12] are included in the download.

We now apply the software to study the effect of stochasticity on equilibrium local dynamics for a pair of example systems, using the homotopy continuation method described in the previous section. The first example is simple enough to be analyzed and presented in full detail. The second example is considerably more complex; the application of MFK tools to it yields some qualitative and quantitative insights, but also suggests questions for further research.

Example 2 (**Numerical Study with MFK for Complex Formation/Dissociation**) The Jacobian of the system in Example 1 is obtained from (33) as

$$\mathbf{J}(z,\mho) = \begin{bmatrix} k_1\left[2\mu_C - (\pi_1+\pi_2)\right] - k_2 & k_1 \\ 4k_1\sigma_{CC} + \frac{1}{\Omega}\left(k_1\left[2\mu_C - (\pi_1+\pi_2)\right] + k_2\right) & 2k_1\left[2\mu_C - (\pi_1+\pi_2)\right] - 2k_2 + \frac{k_1}{\Omega} \end{bmatrix}.$$

The right-hand side of the MFK evolution equations at $\mho = 0$ is

$$g(\mathbf{z},0) = \begin{bmatrix} k_1\left[\pi_1\pi_2 - (\pi_1+\pi_2)\,\mu_C + \mu_C^2 + \sigma_{CC}\right] - k_2\mu_C \\ 2\sigma_{CC}\left(k_1\left[2\mu_C - (\pi_1+\pi_2)\right] - k_2\right) \end{bmatrix}. \tag{40}$$

In what follows, all initial concentrations are set to 15, all rate constants are set to 1, and the conserved concentrations are $\boldsymbol{\pi} = [30, 30]^T$. Setting $d\mu_C/dt = 0$ in the MAK regime yields two possible MAK equilibrium mean concentrations of 25 and 36. However, 36 is not realizable since $\mu_C \leq 30$. Hence the MAK equilibrium is $\bar{\mathbf{z}}_{MAK} = [25, 0]^T$. The Jacobian at this point is

$$\mathbf{J}(\bar{z}_{MAK}, 0) = \begin{bmatrix} -11 & 1 \\ 0 & -22 \end{bmatrix}. \tag{41}$$

This is an upper triangular matrix with eigenvalues equal to its diagonal elements, which are both real and negative. Thus, this is a locally stable equilibrium. A plot of the real and imaginary parts of the eigenvalues with varying $\mho$ is shown in Figure 1. The red line corresponds to the real part of the less stable eigenvalue and the green line to the real part of the more stable eigenvalue; both eigenvalues have zero imaginary parts in the indicated range of $\mho$. The equilibrium is observed to become unstable at $\mho \approx 4.7$.

To picture the bifurcation in the time domain, trajectories are generated for MAK, as well as in stable, marginally stable and unstable MFK regimes. The MAK trajectory is shown in Figure 2, and is consistent with the dominant time constant of $1/11 \approx 0.09$ seconds associated with the eigenvalues in (41). The trajectories for $\mho = 3$, 4.5 and 5 are shown in Figures 3, 4 and 5 respectively. In each figure, a sample SSA trajectory, along with "true" means and standard deviations obtained from an ensemble of 1000 SSA trajectories, is shown. True system behavior is seen to become more stochastic but remain stable with increasing $\mho$. The MFK approximation shows excellent accuracy at $\mho = 3$, but degrades as $\mho$ approaches 4.7, and becomes unstable beyond that. The decreasing stability of MFK as $\mho$ increases (within the regime where MFK is accurate) suggests that small-volume stochasticity has a destabilizing effect on the equilibrium of the real system.

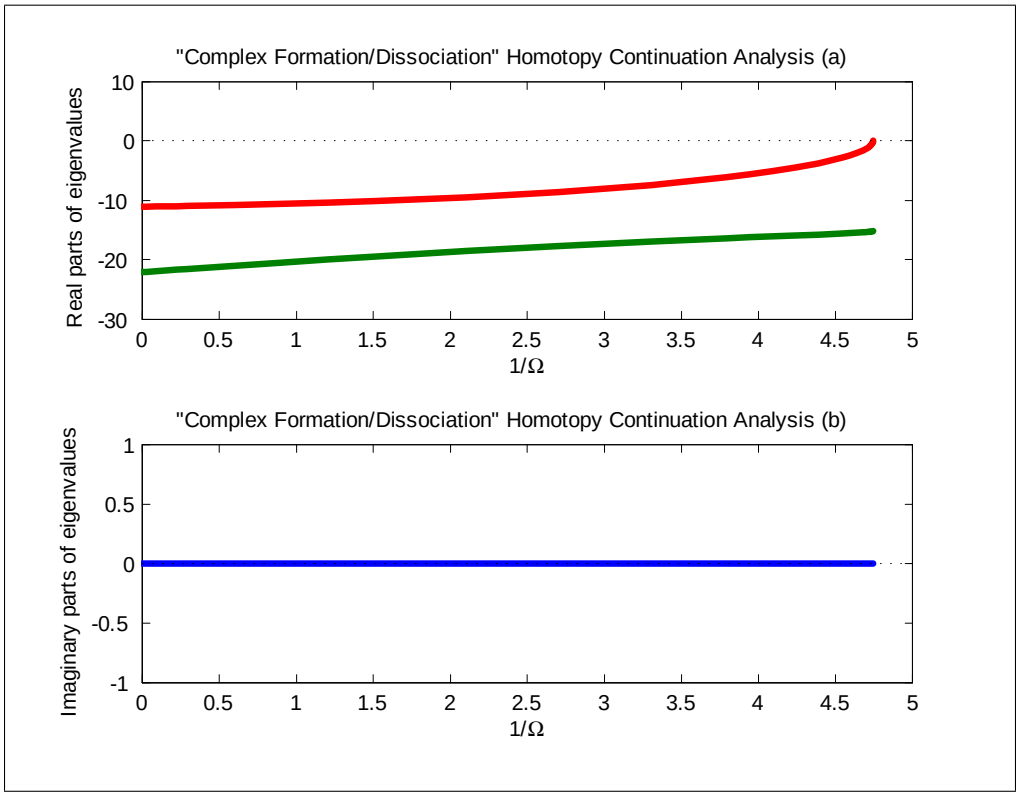

Figure 1: Homotopy continuation analysis results for Example 2.

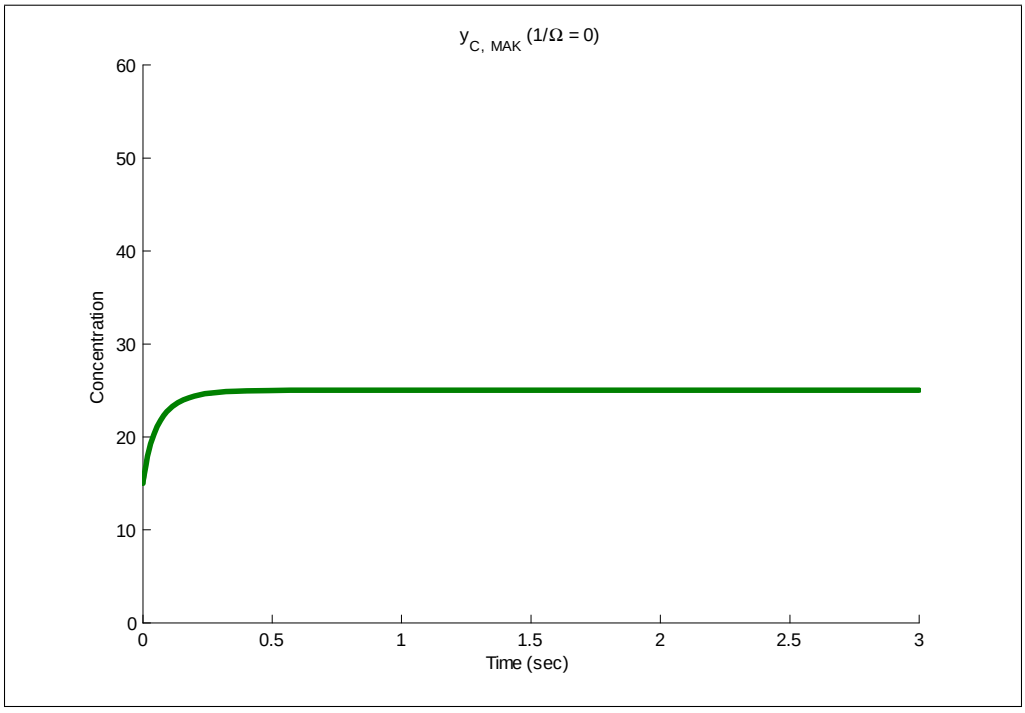

Figure 2: MAK trajectory for Example 2.

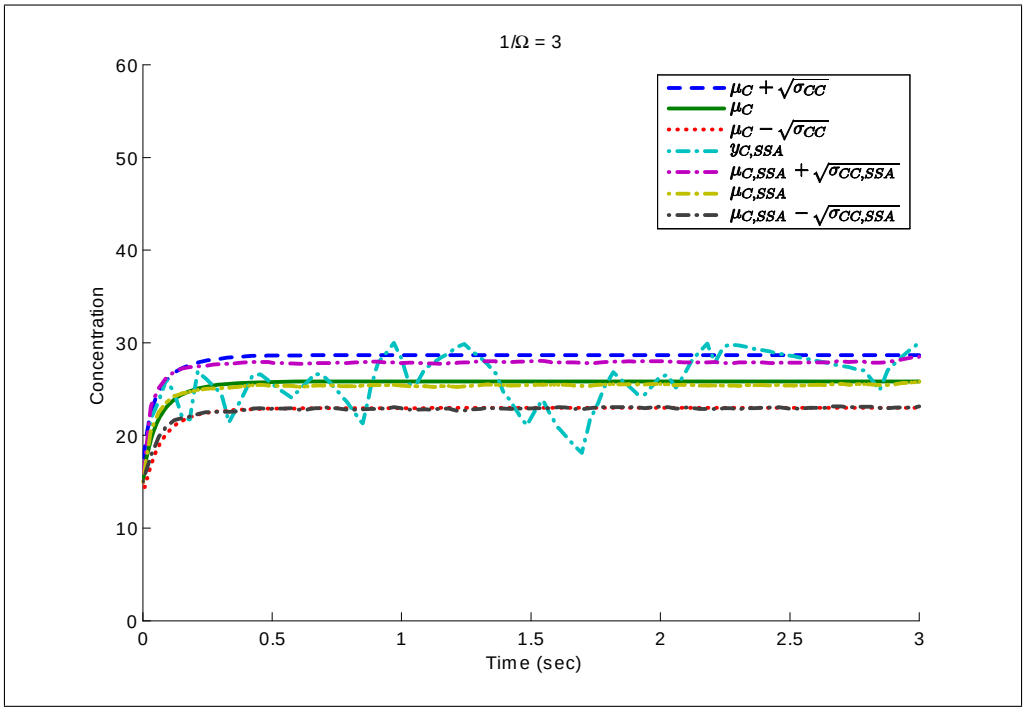

Figure 3: Trajectories in stable MFK regime for Example 2; SSA mean and standard deviation are obtained by averaging over an ensemble of 1000 trajectories.

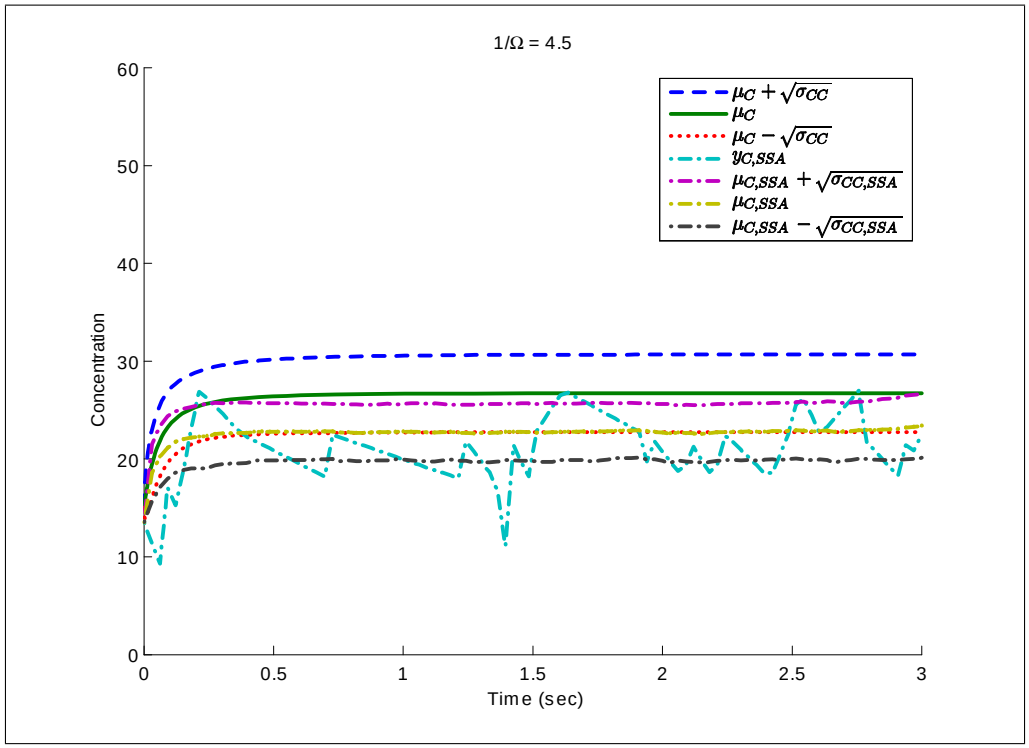

Figure 4: Trajectories in marginally stable MFK regime for Example 2.

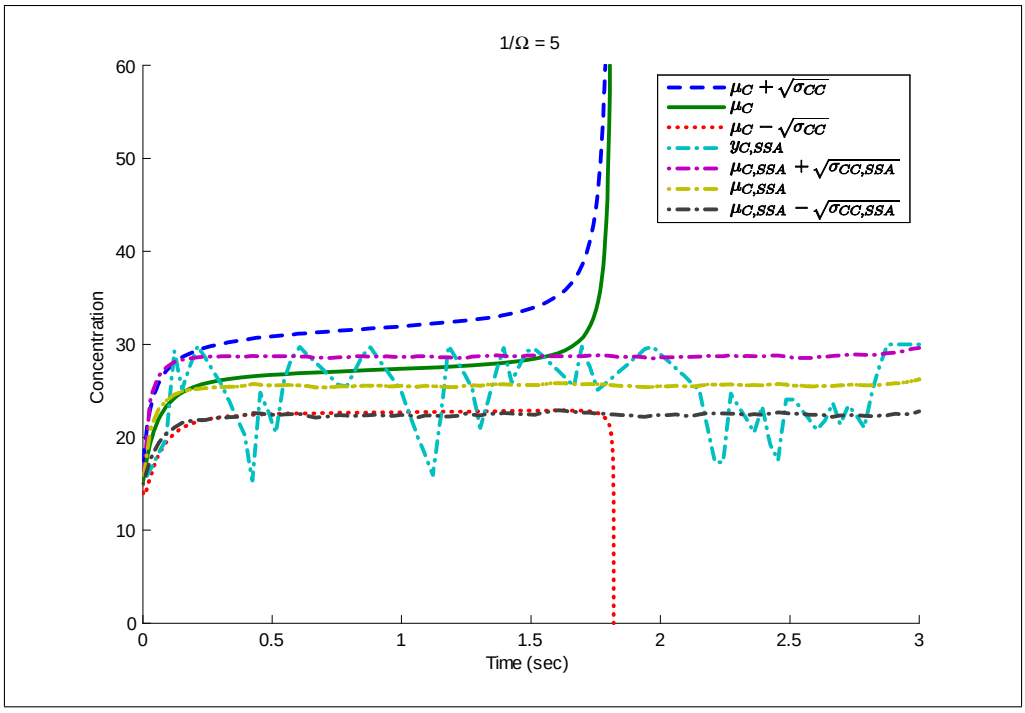

Figure 5: Trajectories in unstable MFK regime for Example 2.

Example 3 (**Numerical Study with MFK for a Genetic Oscillator**) In [18], a genetic oscillator described by the following reactions is presented:

$$X_1 + X_7 \underset{k_2}{\overset{k_1}{\rightleftharpoons}} X_2, \quad X_2 \overset{k_3}{\to} X_2 + X_5, \quad X_1 \overset{k_4}{\to} X_1 + X_5,$$
$$X_3 + X_7 \underset{k_6}{\overset{k_5}{\rightleftharpoons}} X_4, \quad X_4 \overset{k_7}{\to} X_4 + X_6, \quad X_3 \overset{k_8}{\to} X_3 + X_6,$$
$$\varnothing \overset{k_9}{\leftarrow} X_5 \overset{k_{10}}{\to} X_5 + X_7, \quad \varnothing \overset{k_{11}}{\leftarrow} X_6 \overset{k_{12}}{\to} X_6 + X_8,$$
$$X_7 + X_8 \overset{k_{13}}{\to} X_9 \overset{k_{14}}{\to} X_8, \quad X_7 \overset{k_{15}}{\to} \varnothing, \quad X_8 \overset{k_{16}}{\to} \varnothing.$$

This example is also studied in [5]. Here, X_1 and X_3 denote two DNA sequences, X_5 and X_6 denote their respective messenger RNAs, while X_7 and X_8 denote their respective gene products (activator and repressor respectively). Moreover, X_9 denotes the activator-repressor complex, while X_2 and X_4 denote DNA-activator complexes. Initial conditions and parameter values are the same as those listed in Figure 1 of [18], and are not listed in detail here. The system size Ω and maximum initial concentrations were chosen in [18] to be 1, and these values are used in [5] and here.

The MAK description for this set of parameters does not oscillate, as shown in Figure 6, unlike the SSA trajectories, which oscillate for the specified $\mho = 1$ (see Figure 7) as well as for $\mho$ values as low as 0.11 (see Figures 8-10). The SSA trajectories in an ensemble corresponding to a fixed $\mho$ de-synchronize over time, despite having the same initial condition (see Example C of [5] for a more detailed discussion of this point). Accordingly, the ensemble means, computed here from a sample of 100 SSA realizations, show some initial oscillation, but with an amplitude that decays over time. Since the MFK model is an approximation of the ensemble means and covariances, the MFK means should show some oscillatory behavior with decaying amplitude as well (if MFK is at least qualitatively accurate in the corresponding regime). This is the case for $\mho = 0.16$ and 0.11

in Figures 9 and 10. Surprisingly, for $\mho$ values larger than ≈ 0.18 (see Figures 7 and 8), the MFK means instead oscillate with a period and amplitude remarkably close to that of the individual SSA realizations, even though the MFK model is clearly inaccurate for these values of $\mho$.

We use our software to further analyze in an automated fashion the behavior of the MFK model for this high-dimensional system. The eigenvalue locus corresponding to changing system volume from infinity downwards is shown in Figure 11; only the rightmost two eigenvalues are shown, and these have identical real parts, which appears as a single red line in the figure. Here, as in Example 2 (see Figure 1), the real parts of the rightmost eigenvalues become more positive as $\mho$ increases (and in particular the slope of the real parts of the rightmost eigenvalues is positive at $\mho = 0$). This suggests that the MFK model becomes more unstable with decreasing system size. We infer that adding small-volume stochasticity to the macroscopic (MAK) model makes the system equilibrium more unstable locally.

Figure 11 suggests that the MFK model will begin to qualitatively differ from MAK at some value of $\mho$ approaching 0.2 (since at this point the corresponding equilibrium becomes unstable). The trajectories in Figure 8 confirm that this prediction is correct, as MFK begins to oscillate for $\mho \approx 0.18$. For lower values of $\mho$, such as $\mho = 0.16$ in Figure 9, MFK does not oscillate (although it does oscillate twice before settling, perhaps suggesting oscillatory behavior of the ensemble means and the individual SSA trajectories). For even lower values of $\mho$, such as $\mho = 0.11$ in Figure 10, the MFK model oscillates once and then settles. The MFK model is thus quantitatively inaccurate in this regime, as it fails to closely follow the ensemble statistics.

It is worth noting that in general, even for parameter values where individual state trajectories exhibit sustained oscillations, the solution to the master equation (the joint distribution of molecule numbers) will likely reach a constant steady state, leading to steady-state ensemble statistics (like the means, variances and covariances) that are constant. Detecting sustained oscillations in individual state trajectories by analyzing the master equation solution, or any approximation thereof (including SSA ensemble statistics or moment closures like MFK), is thus not straightforward. For such systems, perhaps other ensemble statistics, like the autocorrelations and cross-correlations, might reveal the possibility of sustained oscillations in individual state trajectories.

5 Conclusion

A set of tools to aid in the analysis of systems within the MFK framework has been presented. A closed-form expression for the MFK Jacobian matrix was derived. The application of this expression to the computation of MFK equilibria and their bifurcation analysis was outlined. Software, developed in MATLAB to systematize the analysis of systems within the MFK framework, was presented. Bifurcation analysis was applied to numerically study the effect of small-volume stochasticity on local dynamics at equilibria in a pair of example systems, by focusing on the eigenvalue locus corresponding to decreasing system volume. For both systems, the numerical study revealed volume regimes where MFK provides a quantitatively and/or qualitatively correct description of system behavior, and regimes where the MFK approximation is inaccurate. Our analysis suggests that decreasing volume from the MAK regime (and thus increasing small-volume stochasticity) has a destabilizing effect on system dynamics. That is, the rightmost eigenvalues of the Jacobian evaluated at the macroscopic equlibrium move towards the origin as the system size becomes finite (as our parameter $\mho$ goes from zero to some small value ε).

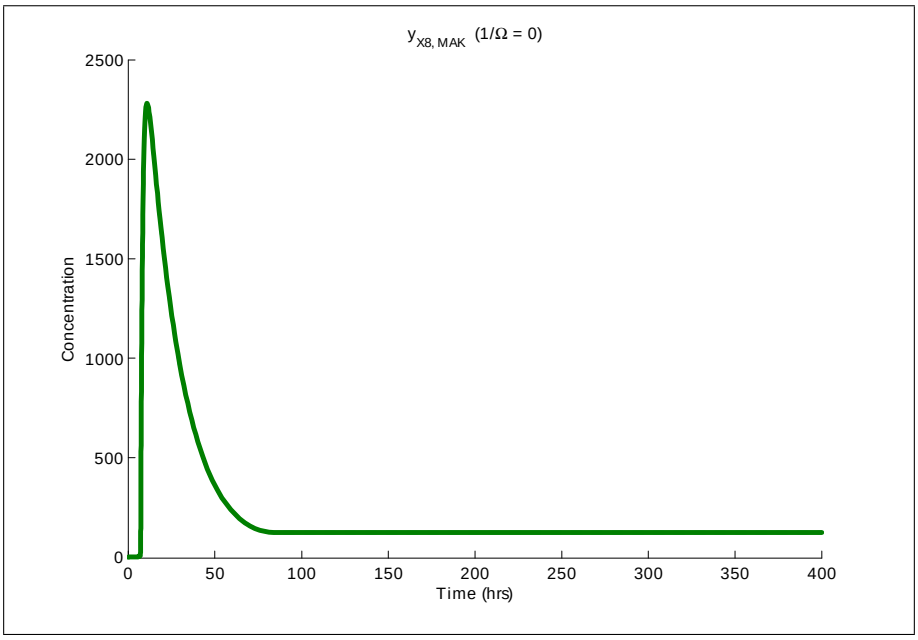

Figure 6: MAK trajectory for Example 3.

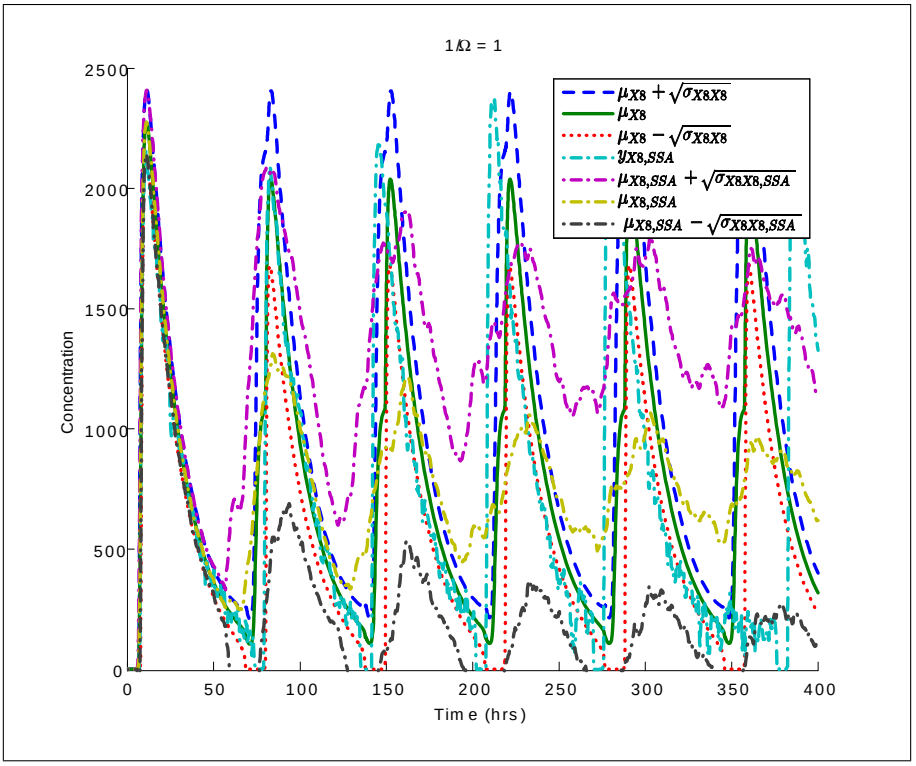

Figure 7: Trajectories in oscillatory MFK regime for Example 3; SSA mean and standard deviation are obtained by averaging over an ensemble of 100 trajectories.

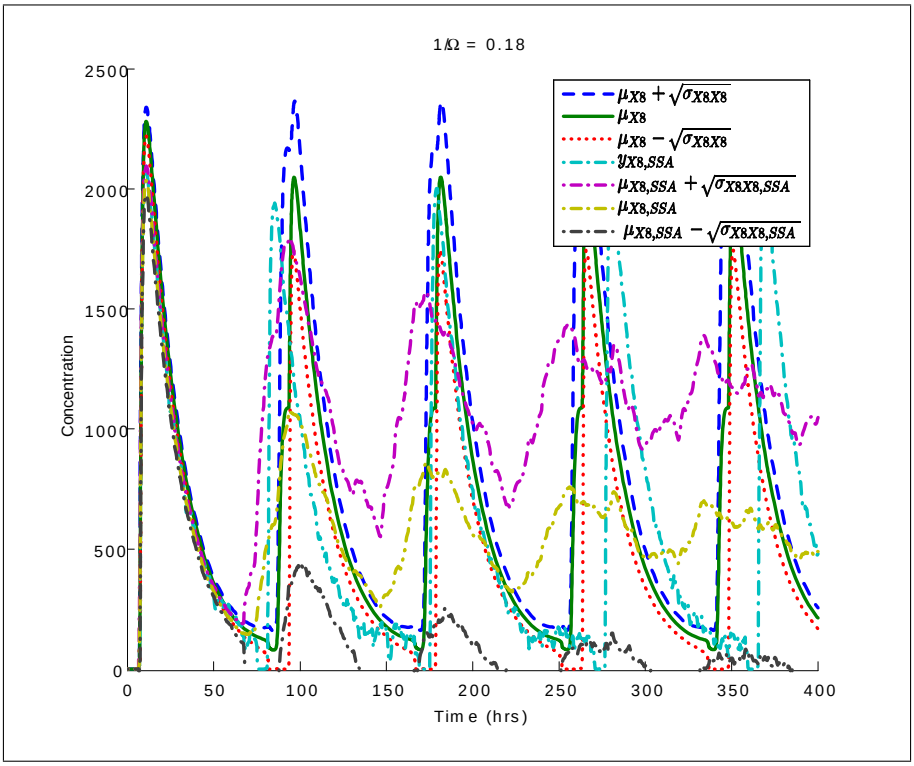

Figure 8: Trajectories in oscillatory MFK regime for Example 3.

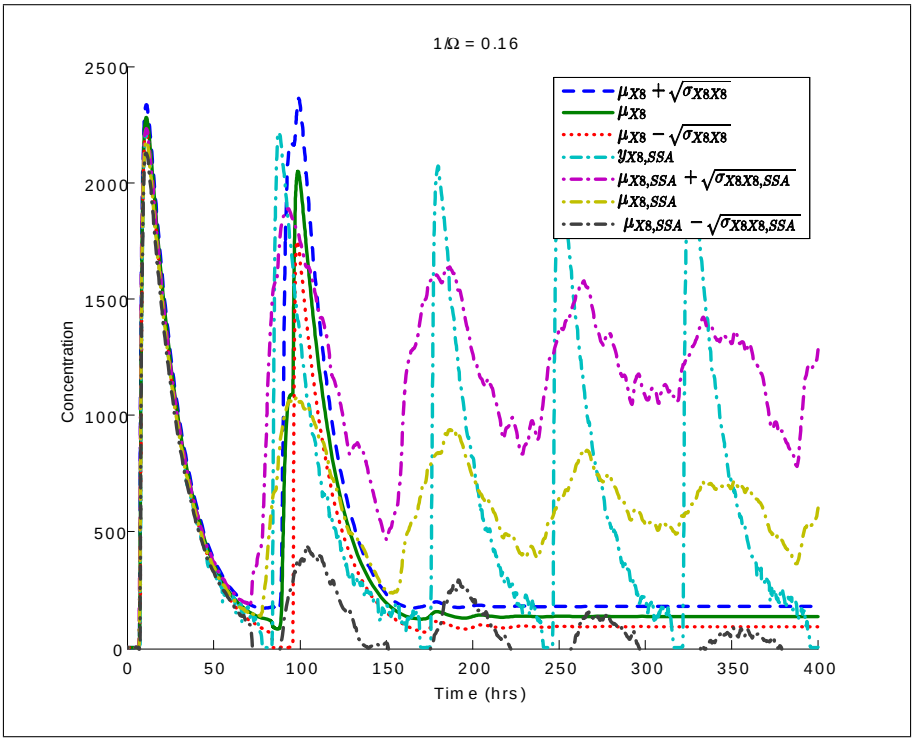

Figure 9: Trajectories in non-oscillatory MFK regime for Example 3.

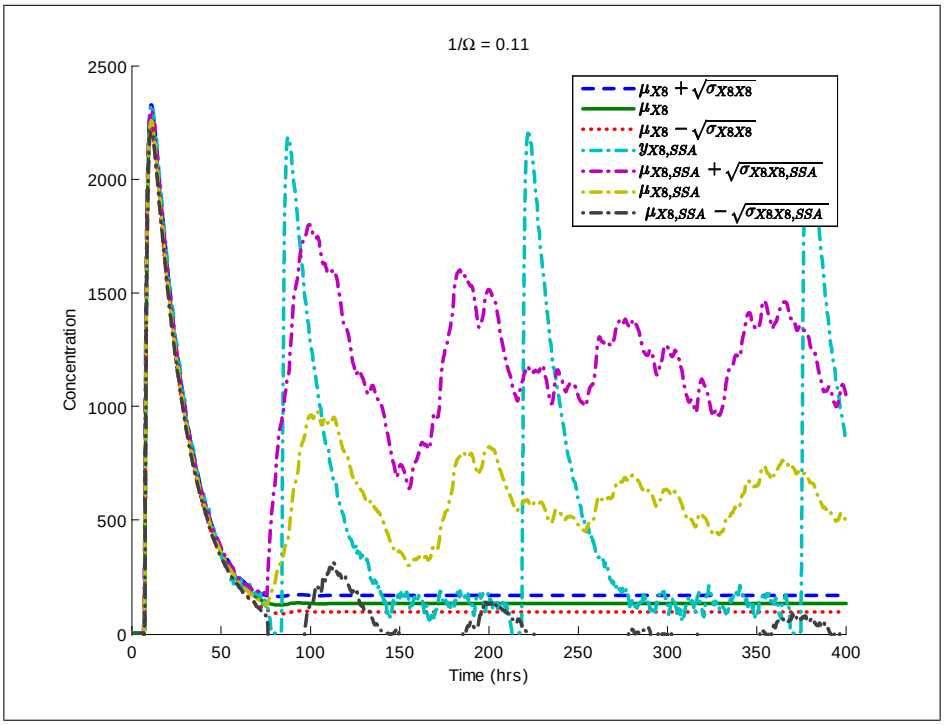

Figure 10: Trajectories in non-oscillatory MFK regime for Example 3.

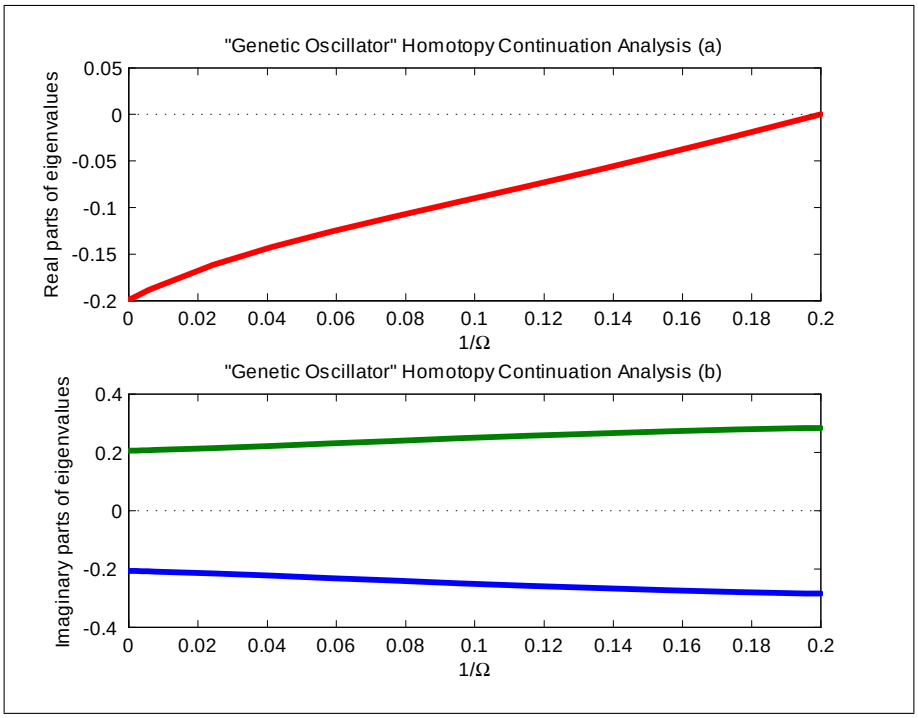

Figure 11: Homotopy continuation analysis results for Example 3.

6 Acknowledgements

The authors would like to thank the anonymous referees for several useful suggestions. They are also grateful to Prof. João Hespanha of UC Santa Barbara for some helpful comments.

A Derivation of the MFK Jacobian Matrix

We first outline the key definitions and identities that are used in the derivation.

The derivative of the scalar $f(\mathbf{h})$ with respect to $\mathbf{h} \in \mathbb{R}^n$ is defined as the gradient vector

$$\frac{df(\mathbf{h})}{d\mathbf{h}} = \left[\begin{array}{ccc} \frac{df(\mathbf{h})}{dh_1} & \cdots & \frac{df(\mathbf{h})}{dh_n} \end{array} \right] \in \mathbb{R}^{1\times n}. \tag{42}$$

Note that $\frac{df(\mathbf{h})}{d\mathbf{h}^T}$ is simply the transpose of the gradient vector above. These definitions are applied element-wise to find the derivative of a vector or matrix function of $\mathbf{h}$.

We use the standard notation $\mathbf{A} \otimes \mathbf{B}$ to denote the Kronecker product of the matrices $\mathbf{A}$ and $\mathbf{B}$, i.e., the block-matrix whose (i,j)th block is $a_{ij}\mathbf{B}$, where a_{ij} is the element of $\mathbf{A}$ in its ith row and jth column. Recall also the definitions of *vec* and *vech* from the beginning of Section 3. The following identities [13], for matrices of compatible dimensions, are useful for algebraic simplification purposes:

$$vec\{\mathbf{A}_1\mathbf{A}_2\mathbf{A}_3\} = \left(\mathbf{A}_3^T \otimes \mathbf{A}_1\right) vec\{\mathbf{A}_2\}, \tag{43}$$

$$(\mathbf{A}_1 \otimes \mathbf{A}_2)(\mathbf{A}_3 \otimes \mathbf{A}_4) = \mathbf{A}_1\mathbf{A}_3 \otimes \mathbf{A}_2\mathbf{A}_4. \tag{44}$$

The first task in deriving the Jacobian it to vectorize the MFK equations (10) for the evolution of the concentration covariance matrix $\mathbf{V}$. (The MFK equations for the evolution of the concentration mean values is already in vector form, namely (9).) Straightforward computations show that

$$\begin{aligned} vec\left\{\frac{d\mathbf{V}}{dt}\right\} = \frac{d\left(vec\{\mathbf{V}\}\right)}{dt} &= vec\left\{\mathbf{M}\mathbf{V} + \mathbf{V}\mathbf{M}^T\right\} + vec\left\{\frac{1}{\Omega}\mathbf{S}\mathbf{\Lambda}\mathbf{S}^T\right\} \\ &= (\mathbf{I}_n \otimes \mathbf{M} + \mathbf{M} \otimes \mathbf{I}_n) vec\{\mathbf{V}\} + \frac{1}{\Omega}(\mathbf{S} \otimes \mathbf{S}) vec\{\mathbf{\Lambda}\}, \end{aligned} \tag{45}$$

from which we get

$$\frac{d\left(vech\{\mathbf{V}\}\right)}{dt} = \mathbf{E}_n(\mathbf{I}_n \otimes \mathbf{M} + \mathbf{M} \otimes \mathbf{I}_n)\mathbf{F}_n vech\{\mathbf{V}\} + \frac{1}{\Omega}\mathbf{E}_n(\mathbf{S} * \mathbf{S})\mathbf{r}, \tag{46}$$

where $*$ denotes the Khatri-Rao product, i.e., the column-wise Kronecker product, [17].

Denoting $vech\{\mathbf{V}\}$ by $\mathbf{v}$, and invoking the preceeding identities as needed, we can now obtain the partial derivative matrices that comprise the four blocks of the Jacobian matrix, as specified by (33):

$$\frac{\partial}{\partial \boldsymbol{\mu}}\left\{\frac{d\boldsymbol{\mu}}{dt}\right\} = \mathbf{S}\frac{\partial \mathbf{r}}{\partial \boldsymbol{\mu}} = \mathbf{M}, \tag{47}$$

$$\frac{\partial}{\partial \mathbf{v}}\left\{\frac{d\boldsymbol{\mu}}{dt}\right\} = \mathbf{S}\frac{\partial \mathbf{r}}{\partial \mathbf{v}}, \tag{48}$$

$$\begin{aligned} \frac{\partial}{\partial \boldsymbol{\mu}}\left\{\frac{d\mathbf{v}}{dt}\right\} &= \frac{\partial}{\partial \boldsymbol{\mu}}\left\{\mathbf{E}_n(vec\{\mathbf{M}\mathbf{V}\} + vec\left\{\mathbf{V}\mathbf{M}^T\right\}) + \frac{1}{\Omega}\mathbf{E}_n(\mathbf{S} * \mathbf{S})\mathbf{r}\right\} \\ &= \mathbf{E}_n\left(\mathbf{V} \otimes \mathbf{I}_n + (\mathbf{I}_n \otimes \mathbf{V})\mathbf{P}_{nn}\right)\frac{\partial\left(vec\{\mathbf{M}\}\right)}{\partial \boldsymbol{\mu}} + \frac{1}{\Omega}\mathbf{E}_n(\mathbf{S} * \mathbf{S})\frac{\partial \mathbf{r}}{\partial \boldsymbol{\mu}}, \text{ and} \end{aligned} \tag{49}$$

$$\frac{\partial}{\partial \mathbf{v}}\left\{\frac{d\mathbf{v}}{dt}\right\} = \mathbf{E}_n(\mathbf{I}_n \otimes \mathbf{M} + \mathbf{M} \otimes \mathbf{I}_n)\mathbf{F}_n + \frac{1}{\Omega}\mathbf{E}_n(\mathbf{S} * \mathbf{S})\frac{\partial \mathbf{r}}{\partial \mathbf{v}}. \tag{50}$$

Here, $\mathbf{P}_{nn}$ is the commutation matrix, defined so that $vec\left\{\mathbf{M}^T\right\} = \mathbf{P}_{nn} vec\{\mathbf{M}\}$ [13].

To specialize the Jacobian to the case of quadratic propensities, we need to explicitly find all necessary derivatives above, using the information in Section 2.3:

$$\begin{aligned}
\frac{\partial \mathbf{r}}{\partial \boldsymbol{\mu}} &= \mathbf{K}\left(\mathbf{C}^T + 2\mathbf{D}^T(\mathbf{I}_n \otimes \boldsymbol{\mu})\right), && (51)\\
\frac{\partial \mathbf{r}}{\partial \mathbf{v}} &= \mathbf{K}\mathbf{D}^T\mathbf{F}_n, && (52)\\
\frac{\partial\left(vec\left\{\mathbf{M}\right\}\right)}{\partial \boldsymbol{\mu}} &= \frac{\partial}{\partial \boldsymbol{\mu}}\left\{vec\left\{2\mathbf{S}\mathbf{K}\mathbf{D}^T(\mathbf{I}_n \otimes \boldsymbol{\mu})\right\}\right\}\\
&= \left(\mathbf{I}_n \otimes 2\mathbf{S}\mathbf{K}\mathbf{D}^T\right)\frac{\partial}{\partial \boldsymbol{\mu}}\left\{vec\left\{\mathbf{I}_n \otimes \boldsymbol{\mu}\right\}\right\}\\
&= \left(\mathbf{I}_n \otimes 2\mathbf{S}\mathbf{K}\mathbf{D}^T\right)\left(vec\left\{\mathbf{I}_n\right\} \otimes \mathbf{I}_n\right). && (53)
\end{aligned}$$

Substituting these expressions into (47), (48), (49) and (50) as appropriate, we get the four block entries of the Jacobian for the case of quadratic propensities to be

$$\begin{aligned}
\frac{\partial}{\partial \boldsymbol{\mu}}\left\{\frac{d\boldsymbol{\mu}}{dt}\right\} &= \mathbf{S}\mathbf{K}\left(\mathbf{C}^T + 2\mathbf{D}^T(\mathbf{I}_n \otimes \boldsymbol{\mu})\right), && (54)\\
\frac{\partial}{\partial \mathbf{v}}\left\{\frac{d\boldsymbol{\mu}}{dt}\right\} &= \mathbf{S}\mathbf{K}\mathbf{D}^T\mathbf{F}_n, && (55)\\
\frac{\partial}{\partial \boldsymbol{\mu}}\left\{\frac{d\mathbf{v}}{dt}\right\} &= \mathbf{E}_n\left(\mathbf{V} \otimes \mathbf{I}_n + (\mathbf{I}_n \otimes \mathbf{V})\,\mathbf{P}_{nn}\right)\left(\mathbf{I}_n \otimes 2\mathbf{S}\mathbf{K}\mathbf{D}^T\right)\left(vec\left\{\mathbf{I}_n\right\} \otimes \mathbf{I}_n\right)\\
&\quad + \frac{1}{\Omega}\mathbf{E}_n(\mathbf{S} * \mathbf{S})\mathbf{K}\left(\mathbf{C}^T + 2\mathbf{D}^T(\mathbf{I}_n \otimes \boldsymbol{\mu})\right), && (56)\\
\frac{\partial}{\partial \mathbf{v}}\left\{\frac{d\mathbf{v}}{dt}\right\} &= \mathbf{E}_n(\mathbf{I}_n \otimes \mathbf{M} + \mathbf{M} \otimes \mathbf{I}_n)\mathbf{F}_n + \frac{1}{\Omega}\mathbf{E}_n(\mathbf{S} * \mathbf{S})\mathbf{K}\mathbf{D}^T\mathbf{F}_n. && (57)
\end{aligned}$$

References

[1] Elowitz, M. B.; Levine, A. J.; Siggia, E. D.; Swain, P. S. *Science* **2002**, *297*(5584), 1183–1186.

[2] Gillespie, D. T. *Annu Rev Phys Chem* **2007**, *58*, 35–55.

[3] Kampen, N. V. *Stochastic Processes in Physics and Chemistry;* Elsevier, **2001**.

[4] Paulsson, J. *Physics of Life Reviews* **2005**, *2*(2), 157–175.

[5] Gómez-Uribe, C. A.; Verghese, G. C. *The Journal of Chemical Physics* **2007**, *126*(2), 024109.

[6] Goutsias, J. *Biophysical Journal* **2007**, *92*(7), 2350–65.

[7] Whittle, P. *Journal of the Royal Statistical Society B* **1957**, *19*(2), 268–281.

[8] Singh, A.; Hespanha, J. *IEEE Trans. Automatic Control* **2011**, *56*(2), 414–418.

[9] Gallager, R. G. *Discrete Stochastic Processes;* Kluwer Academic Publishers, **1995**.

[10] Gillespie, C. S. *IET Systems Biology* **2009**, *3*(1), 52–58.

[11] Lee, C. H.; Kim, K.-H.; Kim, P. *The Journal of Chemical Physics* **2009**, *130*(13), 134107–134115.

[12] Azunre, P. Mass fluctuation kinetics: Analysis and computation of equilibria and local dynamics, Master's thesis, EECS Dept., Massachusetts Institute of Technology, **2009**.

[13] Magnus, J. R.; Neudecker, H. *Matrix Differential Calculus with Applications in Statistics and Econometrics;* John Wiley & Sons, 2nd ed., **1999**.

[14] Tolsma, J. E.; Barton, P. I. *Computers & Chemical Engineering* **1998**, *22*(4-5), 475–490.

[15] Ortega, J. M.; Rheinboldt, W. C. *Iterative Solution of Nonlinear Equations in Several Variables;* Society for Industrial and Applied Mathematics: Philadelphia, PA, USA, **2000**.

[16] Scott, M.; Hwa, T.; Ingalls, B. *Proceedings of the National Academy of Sciences* **2007**, *104*(18), 7402–7407.

[17] Liu, S. *Linear Algebra and its Applications* **1999**, *289*, 267–277.

[18] Vilar, J. M.; Kueh, H. Y.; Barkai, N.; Leibler, S. *Proceedings of the National Academy of Sciences* **2002**, *99*(9), 5988–5992.